Available online at www.sciencedirect.com
ScienceDirect
Journal of Power Sources 168 (2007) 400–407
JOURNAL OF POWER SOURCES
www.elsevier.com/locate/jpowsour

Effects of humidification temperatures on local current characteristics in a PEM fuel cell

Hong Sun [a,b], Guangsheng Zhang [a], Lie-Jin Guo [a], Shang Dehua [a], Hongtan Liu [a,c,*]

[a] State Key Laboratory of Multiphase Flow in Power Engineering, Xi'an Jiaotong University, Xi'an, Shanxi 710049, China
[b] Trasportation and Mechanical Engineering Faculty, Shenyang Jianzhu University, Shenyang Liaoning 110168, China
[c] Department of Mechanical and Aerospace Engineering, P.O. Box 248294, University of Miami, Coral Gables, FL 33124, USA

Received 1 February 2007; received in revised form 7 March 2007; accepted 8 March 2007
Available online 15 March 2007

Abstract

It is well known that water plays a very important role in the performance of proton exchange membrane (PEM) fuel cells. Non-uniform water content in the membrane leads to non-uniform ionic resistance, and non-uniform liquid water fraction in the porous electrode causes varied mass transfer resistances. The objective of this work is to study the effects of different anode and cathode humidification temperatures on local current densities of a PEM fuel cell with a co-flow serpentine flow field. The method used is the current distribution measurement gasket technique [H. Sun, G.S. Zhang, L.J. Guo, H. Liu, J. Power Sources 158 (2006) 326–332]. The experimental results show that both air and the hydrogen need to be humidified to ensure optimal cell performance, and too high or too low humidification temperature can cause severe non-uniform distribution of local current density. From the experimental results of local current density distributions, the local membrane hydration, the optimal humidification temperature, and if flooding occurs can be obtained. Such detailed local measurement results could be very valuable in fuel cell design and operation optimizations.

Keywords: PEM; Fuel cell; Current distribution

1. Introduction

Water management is critical in PEM fuel cell performances. It is well known that the currently used commercial polymer electrolyte membrane in PEM fuel cells must be well hydrated to maintain high proton conductivity. Yet, excessive liquid water can cause flooding of the pores in catalyst layers and the gas diffusion layers (GDL), thus causing higher mass transfer resistance to the reactants. This is especially true on the cathode side, since water is produced in the cathode catalyst layer and water is also transferred from the anode to the cathode due to electro-osmosis. Due to the conflicting roles of water, proper gas humidification is very important to ensure high cell performances. The balance of water is made more complicated by the fact that water content in the membrane and liquid water distribution in the electrode are not uniform. The non-uniform distributions of water lead to non-uniform distribution of current density.

Recently, various techniques have been developed to measure local current densities in PEM fuel cells. Wieser et al. [2] developed a technique using a magnetic loop array to measure current distribution in PEM fuel cell. In this technique, the current collector of the fuel cell was modified. Stumper et al. [3] measured the current distribution using a partial membrane electrode assembly method, a sub-cell method, and a current mapping technique. Cleghorn et al. [4] demonstrated a printed circuit board technology to measure current distribution in PEM fuel cells. In this technique, the current collector and flow field of fuel cell were segmented. A similar approach to the printed circuit board technique was used by Brett [5] to investigate the current density distribution in PEM fuel cell. Geiger et al. [6] described a new magnetic loop array with closed-loop Hall Effect current sensors to measure current distribution in a PEM fuel cell. The segmented flow field approach [7] and its derivatives [8] were popular techniques in measuring current distributions. Hakenjos

* Corresponding author at: Department of Mechanical and Aerospace Engineering, P.O. Box 248294, University of Miami, Coral Gables, FL 33124, USA. Tel.: +1 305 284 2019; fax: +1 305 284 2580.
E-mail address: hliu@miami.edu (H. Liu).

0378-7753/$ – see front matter © 2007 Elsevier B.V. All rights reserved.
doi:10.1016/j.jpowsour.2007.03.022

et al. [9] developed a segmented anode flow field approach to measure the current distribution in PEM fuel cells. Liu et al. [10] measured the current density distribution in PEM fuel cell using a sub-cell method. A segmented cell structure technique [11] was developed to determine the current density distribution in an operating PEM fuel cell. Sun et al. [1] developed a technique using a current measuring gasket and the results showed that the operating parameters have complicated effects on local current density distributions as well as cell performances.

Various mathematical models that incorporating liquid water were also developed for PEM fuel cells. Wang et al. [12] and You and Liu [13] developed two-dimensional, two-phase flow models to investigated water and oxygen transfer in the cathode of PEM fuel cell. Natarajan and Nguyen [14] and Hu et al. [15,16] developed three-dimensional, two-phase flow models to studied liquid water transfer in PEM fuel cells. Sun et al. [17] also developed a two-dimensional, two-phase flow model to investigate the effects of operating parameters, especially the humidification temperature, on liquid water transport in the cathode of PEM fuel cells.

There is a limited number of experimental studies that deal with the effects of humidification temperatures on local current density [1,4,11], but there is no systematic study of effects of gas humidification temperature on the local current density distributions, and yet such information is very valuable in understanding the true effects of humidification and in determining the optimal operating conditions. In this work, the effects of humidification temperature on local current density distribution in a PEM fuel cell with a co-flow serpentine flow field are systematically studies.

2. Experimental

2.1. Current distribution measurement system

A flow diagram of the current distribution measurement experimental system is shown in Fig. 1. This system consists of a fuel cell test system, a single fuel cell, a current distribution measuring gasket and a multi-channel potentiostat. Cell temperature, humidification temperature, reactant gas flow rate and backpressure are controlled by the fuel cell test system.

The fuel cell test system is controlled by a Labview^{TM}-based application software, which regulates reactant gas flow rates, fuel cell operating temperature, reactant humidification temperature, and operating pressure. Hydrogen and air/oxygen flow rates are controlled by two mass flow controllers, and their respective humidity is controlled by regulating the temperatures of the humidifiers. The operating pressures are regulated by adjusting the backpressure regulators. A nitrogen purging system is incorporated into the experimental system to purge both the anode and cathode sides before and after experiments to ensure safety. Local currents are measured by the multi-channel potentiostat and its control system. The currents from the 23 measuring strips are measured by a 24-channel high-resolution potentiostat, which is controlled by a separate computer system using the MITS Pro^{TM} software.

In this study, a single PEM fuel cell with an active area of 16 cm^2 was used. The membrane used was Nafion^{TM} 112 with a thickness of 53 μm; the platinum catalyst loadings were 0.4 mg/cm^2 on both sides. The gas diffusion layers (GDLs) were carbon fiber paper with 375 μm thickness. The flow field plates were made of graphite, the flow fields were serpentine on both sides. The end plates were made of copper. Detailed information of the fuel cell used is listed in Table 1.

2.2. Current distribution measurement gasket

Fig. 2 shows the schematic diagram of the current distribution measurement gasket. The current distribution measurement gasket consists of a gasket with a pattern of the flow field used in the fuel cell. The substrate of the gasket is made of epoxy resin and glass cloth, the top surface is plated with copper and gold, and the measuring strips extend out of the cell for individual current collection.

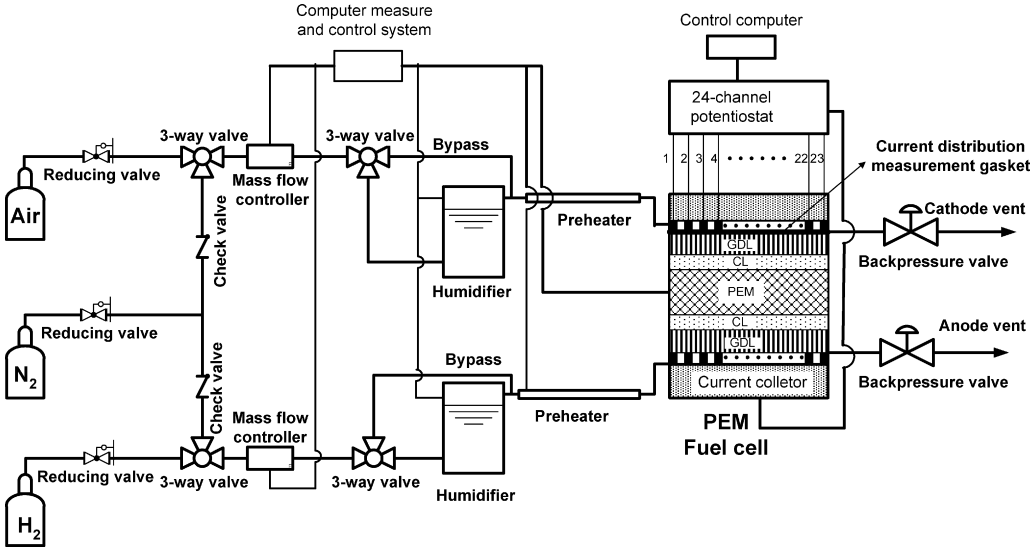

Fig. 1. Schematic of experimental system.

Table 1
Geometric parameters of the experimental fuel cell

Active area (cm^2)	16.0
Channel length (cm)	4.0
Channel width (cm)	0.075
Channel depth (cm)	0.095
Number of channels	24
Gas diffuser thickness (cm)	0.0375
Catalyst layer thickness (cm)	0.00129
Membrane thickness (cm)	0.0053

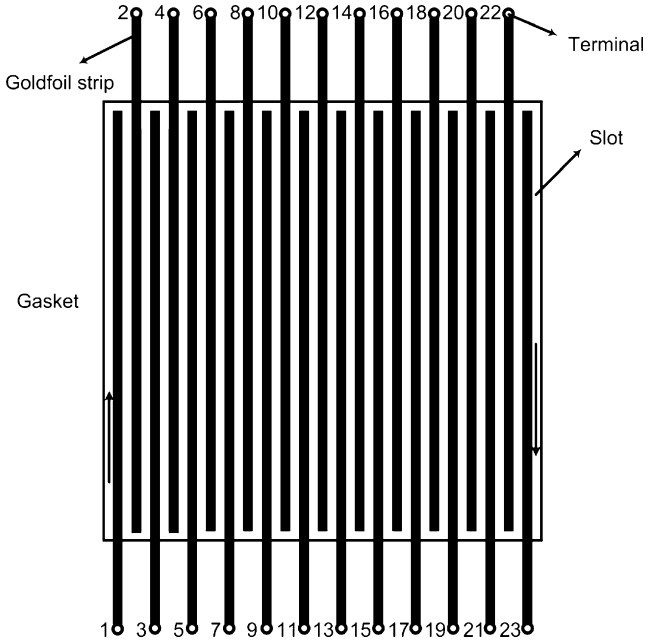

Fig. 2. Schematic diagram of current distribution measurement gasket.

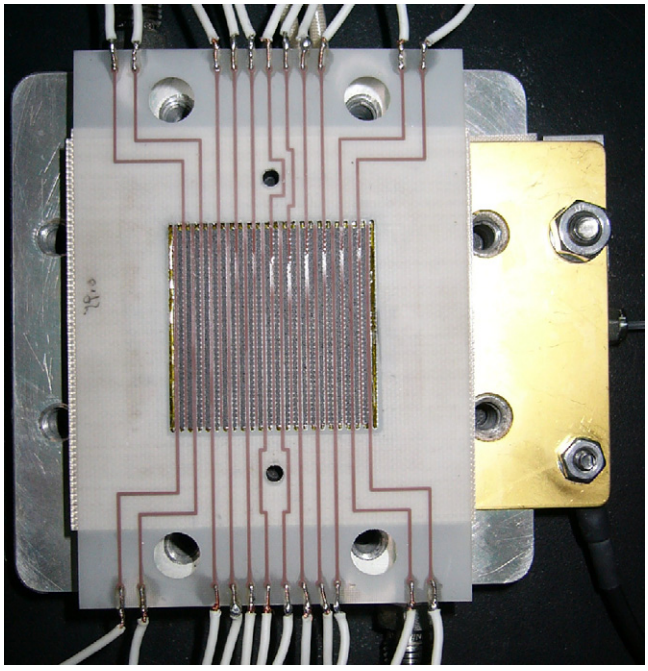

Fig. 3. A photograph of the current distribution measurement gasket.

Table 2
Geometric parameters of the current distribution gasket

thickness of gasket (mm)	0.2
Length of gasket (mm)	106
Width of gasket (mm)	86
Length of single slot (mm)	40
Length of slot (mm)	1000
Width of slot (mm)	0.75
Number of single slot	24
Width of shoulder (mm)	0.83
Number of shoulder	23
Thickness of copper (mm)	0.03
Width of copper (mm)	0.83
Length of copper (mm)	70
Thickness of gold (mm)	0.002
Width of gold (mm)	0.083
Length of gold (mm)	70

The measurement gasket with 23 measuring strips used in this study is as shown in Fig. 3. The overall dimension of the gasket is 10.6 cm long, 8.6 cm wide and 0.2 mm thick. The slots in the measurement gasket corresponding to flow channels in the flow field plate are 0.75 mm wide, and the strips corresponding to the shoulders in the flow field plate are 0.83 mm wide and 40 mm long. All strips are first plated with copper and then gold. The thickness of the copper is 30 μm and that of gold is 2 μm. Detailed information of the current distribution gasket used is listed in Table 2.

The PEM fuel cell used in the experiments is a single fuel cell with an active area of 16 cm^2. The flow field is single-channel serpentine, with 23 shoulders. The dimension of the flow field plate is 8.6 cm × 8.6 cm. The width of the flow channels is 0.92 mm and the depth is 1 mm. The width of the shoulders is 0.83 mm and the length is 40 mm. The total length of the serpentine flow channel is 1000 mm. The flow field in the anode is identical to that in the cathode and parallel flow (co-flow) is used in all the experiments reported in this study.

2.3. Installation of the current distribution measurement gasket

The current measurement gasket is inserted between the flow field plate and the cathode gas diffusion layer, with the gold plated surface in direct contact with the gas diffusion layer. Since the substrate is made of epoxy resin and glass cloth, the measuring strips are insulated from each other and from the flow field; thus, the fuel cell is electrically divided into 23 local areas. The current from the 23 measuring strips are conducted out of the fuel cell laterally instead of to the shoulders of the flow field plate. Two alignment holes and careful cell assembly ensures good alignment of the measuring strips with the collector plate shoulders. In addition, uniform compression is maintained to minimize errors due to non-uniform contact resistance.

3. Results and discussion

The 23 measuring strips are numbered sequentially from the channel inlet to the outlet as shown in Fig. 2. Since the current

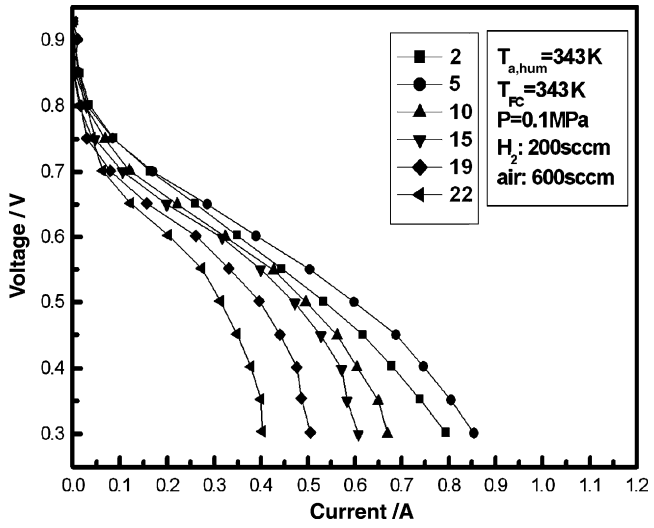

Fig. 4. Selected local polarization curves from inlet to outlet, with anode humidification temperature equal to the cell operating temperature and no cathode humidification.

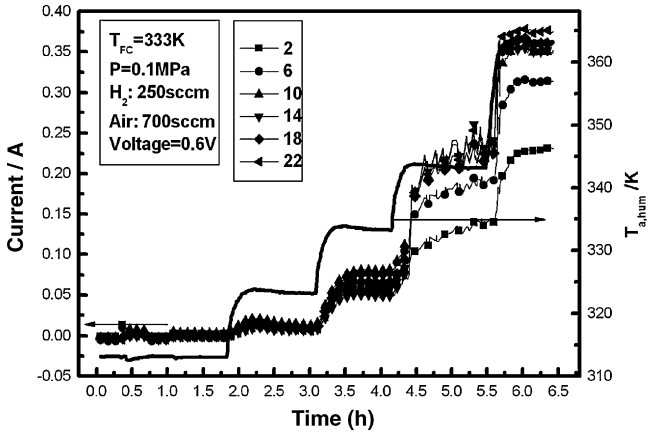

Fig. 5. Selected local current variations as the anode humidification temperature is progressively increased and with no cathode humidification.

density gradient across the fuel cell is small, symmetry can be assumed. Thus, each measuring strip measures the current from a local area covering one shoulder and two half-channels, except numbers 1 and 23, which cover an area of one shoulder plus one and one-half of a channel. Therefore, only the current data from strips 2 to 22 are used in the following presentations. Even though the current data from numbers 1 and 23 are not used in the final result analysis, these two strips must be put in place and connected to the same potentiostat to ensure the validity of the symmetry assumption for the two adjacent measuring strips.

3.1. Anode humidification temperature

Fig. 4 shows a set of local polarization curves for an experiment when the anode humidification temperature is set to be the same as the cell temperature and no cathode humidification. To avoid overcrowding the figure, only six representative polarization curves are plotted instead of the entire twenty one. It is shown in Fig. 4 that the performances of local areas are better near the inlet and then decrease along the gas channel. Since there is no cathode humidification, near the inlet, the membrane is not fully hydrated and the degree of hydration increases along the channel due to both electro-osmosis and water production at the cathode. Thus the local current density also increases along the channel near the inlet. Further along the channel, once the membrane reaches its full hydration, any additional water will not have any positive effect. However, the reactant concentration decreases along the channel due to consumption and causes the local current density to decrease. The resultant effect of the membrane hydration and reactant consumption cause the local performance to increase first and then decrease along the channels.

Fig. 5 shows the variations of local currents as the anode humidification temperature progressively increases with no cathode humidification. The total duration of this experimental run was 6.5 h and no cathode humidification was provided throughout this experiment. From 0 to 0.5 h, no anode humidification was provided and all local currents were essentially zero due to the dry membrane. From 0.5 to 1.65 h, the anode humidification temperature was 313 K, and all the local currents were still essentially zero. In this case, the humidity was too low to hydrate the membrane. From 1.65 to 6.5 h, the anode humidification temperature was increased from 323 to 363 K in three steps. It can be seen from Fig. 5 that all local currents increase with the increase of anode humidification temperature from 323 to 363 K. This is due to the fact that as the anode humidification temperature increases, more and more water is brought into the fuel cell with hydrogen. Thus the water content in the membrane progressively increases and the ionic resistance of the membrane decreases accordingly. It can also be seen that the local current always increases along the flow direction and the highest local current always occurs near the gas exit. This result indicates that the membrane never reach full hydration even when the anode humidification temperature was as high as 363 K. It can be concluded that the water brought in with hydrogen was not enough to humidify the fuel cell and that the product water played a very important role in hydrating the membrane. The accumulative effect of product water caused the increase of current along the flow direction and the effect of the decrease of reactant concentration on the local current was not dominant.

Fig. 6 shows the current distribution from inlet to the exit when the cathode humidification temperature is equal to the cell temperature of 343 K and at various different anode humidification temperatures. For each anode humidification temperature, the overall trend for the local current is to decrease along the gas channel. This is mainly due to the reactant concentration decrease and possible local flooding. For the cases with no or low anode humidification temperatures, the local current density are high at the inlet and decreases steadily along the channel, indicating that anode humidification is not critical when the cathode is highly humidified. When the anode humidification temperature is higher than the cell temperature, the cell currents are lower from the inlet and stay lower than other cases. This result shows that flooding probably exist in the whole cell.

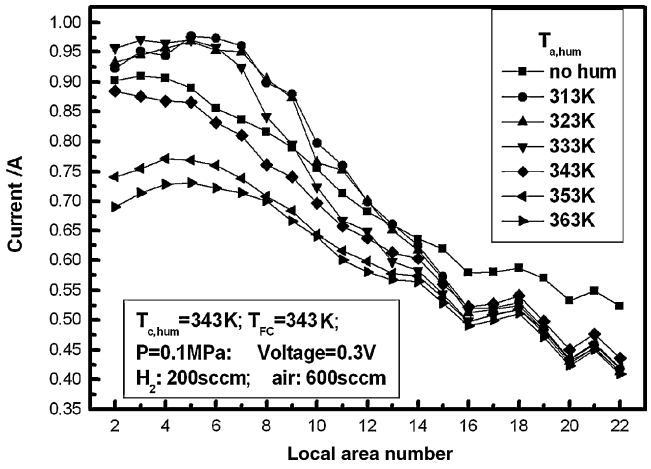

Fig. 6. Current variations along the channel at different anode humidification temperatures and cathode humidification temperature equal to the cell temperature.

3.2. Cathode humidification temperature

Fig. 7 shows selected local polarization curves for the case with no anode humidification and a cathode humidification temperature equal to the cell temperature of 343 K. The trend of local performance variation is similar to that shown in Fig. 4. With only cathode humidification, water in the fuel cell comes from product water and cathode gas stream. Comparing Fig. 7 with Fig. 4, it is found that all local performances shown in Fig. 7 are better than those shown in Fig. 4. This is due to the fact that greater mount of water is introduced into the fuel cell due to a higher air flow rate than that of hydrogen.

Fig. 8 shows selected local current variations as the cathode humidification temperature is progressively increases with no anode humidification. The experiment was carried out for 4.5 h. From 0 to 0.5 h, both air and hydrogen were not humidified, and from 0.5 to 4.5 h, only air was humidified. Local currents were close to zero before 0.5 h due to a dry membrane. The local

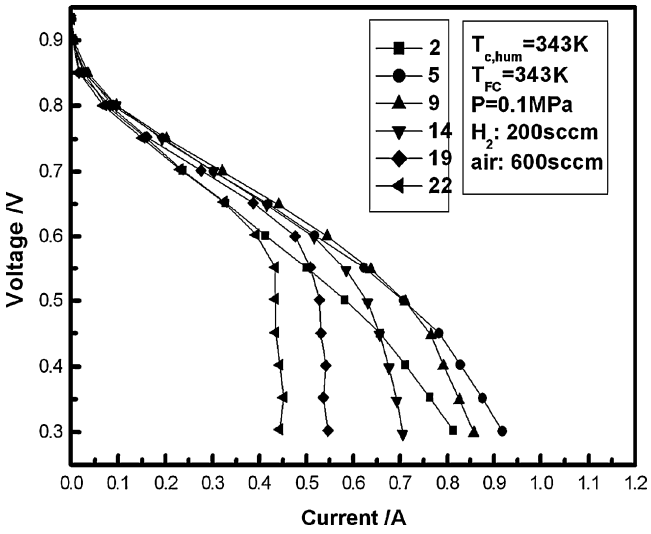

Fig. 7. Selected local polarization curves for no anode humidification and cathode humidification temperature equal to the cell temperature.

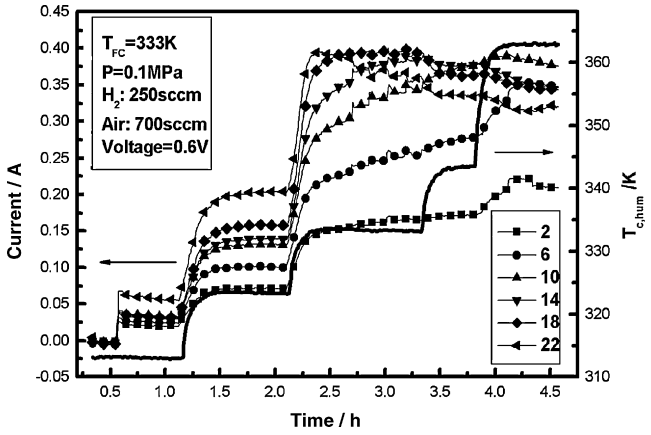

Fig. 8. Selected local current variations as the cathode humidification temperature is progressively increased and with no anode humidification.

currents increased with the increase of cathode humidification temperature from 313 to 333 K because more and more water was brought into the fuel cell with the humidified air, leading to a better hydrated membrane. For cathode humidification temperature from 343 to 363 K, local currents from area 2 to 10 increased with the humidification temperature. This indicates that, even with a cathode humidification temperature higher than the cell temperature, if the anode gas stream is not humidified, the membrane near the inlet of the cell is still not fully hydrated. On the other hand, at such high cathode humidification temperatures, the current in later part of the cell (e.g. area 14–22) decrease with the increase in humidification temperature, indicating the excessive water caused flooding.

From both Figs. 5 and 8, it is clear that in order to obtain optimal cell performance, both anode and cathode need to be humidified and the humidification temperature should be close to the cell temperature but not exceeding it.

Fig. 9 shows the local current variations at different cathode humidification temperatures and the anode humidification temperature was kept equal to the cell temperature. The general

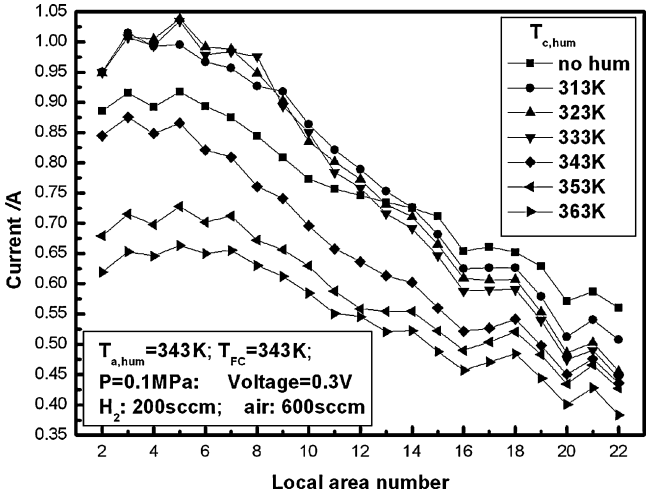

Fig. 9. Current variation along the channel at different cathode humidification temperatures and anode humidification temperature equal to the cell temperature.

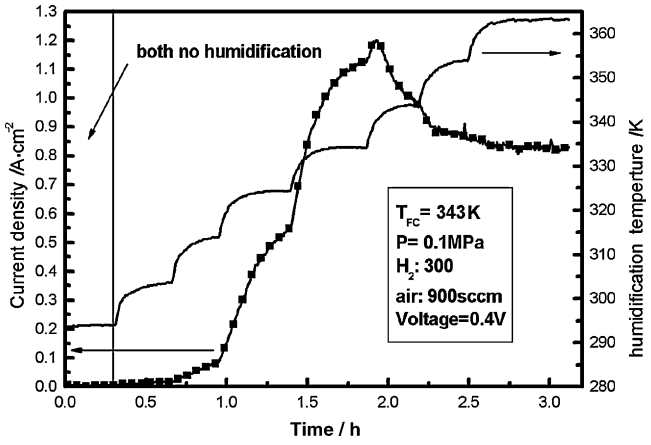

Fig. 10. Transient total cell current variations as the humidification temperatures of both sides are progressively increased.

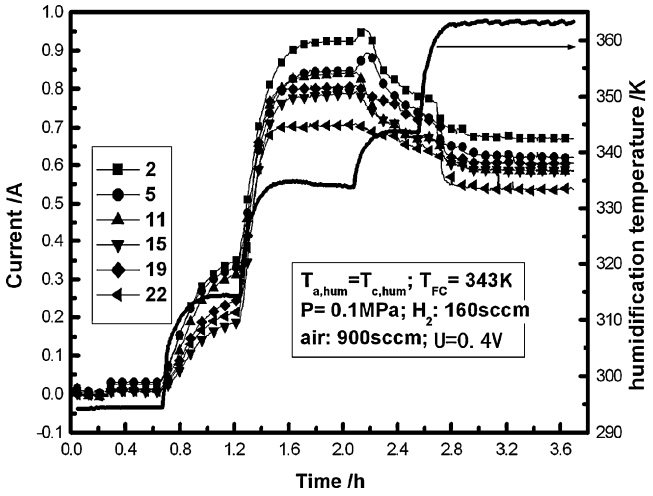

Fig. 11. Transient current distributions for selected locations as the humidification temperature of both sides progressively increases.

trend of current distribution in Fig. 9 is similar to that shown in Fig. 6 for varying anode humidification temperatures. It is interesting to note that, though no or low humidification is not as good as proper humidification, over-humidification is much worse. When the cathode humidification temperature is only 10 K higher than the cell temperature, the performance is significantly lower, indicating that flooring is a very severe and sensitive problem.

3.3. Equal cathode and anode humidification temperature

Fig. 10 shows the total current variations as the humidification temperatures at both sides were progressively increased. To begin with, no humidification was provided and then the humidification temperature was increased from 293 to 363 K as indicated by the solid line in Fig. 10. The total current was essentially zero for no humidification and remained extremely low till the humidification temperatures reached 313 K. Then the current increased with the increase of humidification temperature until 333 K, 10 K below the cell temperature. When the humidification temperature was increase to 343 K, equal to the cell temperature, the cell performance started to deteriorate. Further increase in humidification temperature caused the cell current to further reduce. However, when the humidification was further increased, the rate of cell current reduction decreased.

The experiment for Fig. 11 was similar to that for Fig. 10 except that the durations at each humidification temperature were longer and each individual local current was collected. Again, only selected local currents were plotted in Fig. 11 to avoid cluttering the figure. For all the locations, current increased with humidification temperature till 333 K, 10 K below the cell temperature, and at all locations, current decreased with further increase in humidification temperature. It is interesting to note, though, the deterioration was much more severe at the inlet, indicating flooding started from the inlet.

Fig. 12 shows the local current distributions at different cell voltages when the humidification temperatures at both sides were at 293 K, 40 K lower than the fuel cell operating temperature of 333 K. At a high voltage of 0.7 V, currents at all locations were almost zero due to the dry membrane. At lower cell voltages, local currents were lowest at the inlet and increase monotonously along the gas channel up to the exit, indicating that the membrane never reached full hydration. At such a low humidification temperature, very little water was brought in with the gas streams and membrane around the inlet was very dry. Along the gas channel, more and more water was produced and the membrane became better and better hydrated. This result shows that when operating at very low humidification temperature, the product water plays a critical role in hydrating the membrane and maintaining cell operations.

Fig. 13 is similar to Fig. 12 except that the humidification temperatures were 313 K, 20 K below the fuel cell operating temperature. It can be seen from Fig. 13 that for all the voltages except 0.7 V, the local currents were low at the inlet, increased along the channel, reached a maximum, and then decreased further down the stream. At the inlet, the degree of membrane hydration was low and current was low; along the channel, more and more water wass produced and the membrane hydration

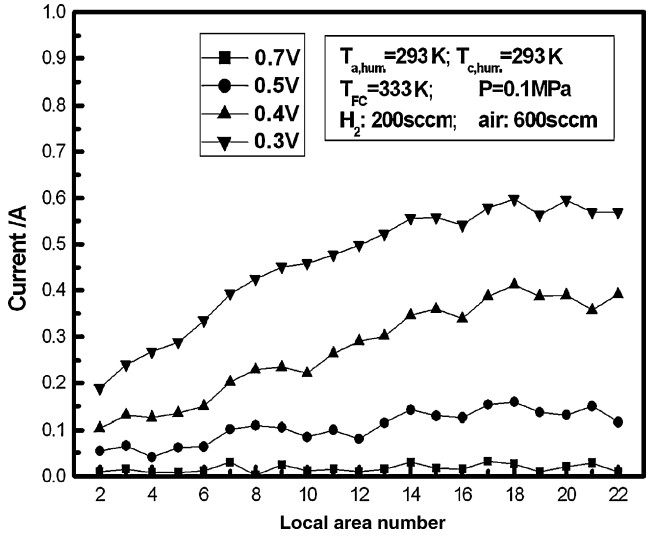

Fig. 12. Local current distributions at different cell voltages. Cell temperature is 333 K, and humidification temperatures at both sides are 293 K.

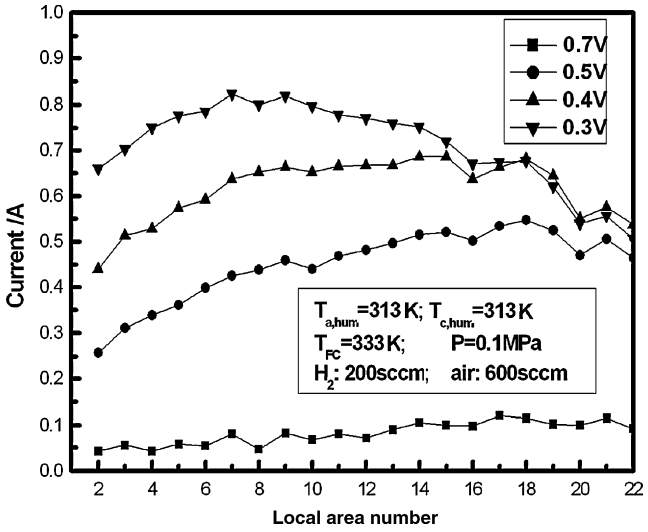

Fig. 13. Local current distributions at different cell voltages. Cell temperature is 333 K, and humidification temperatures at both sides are 313 K.

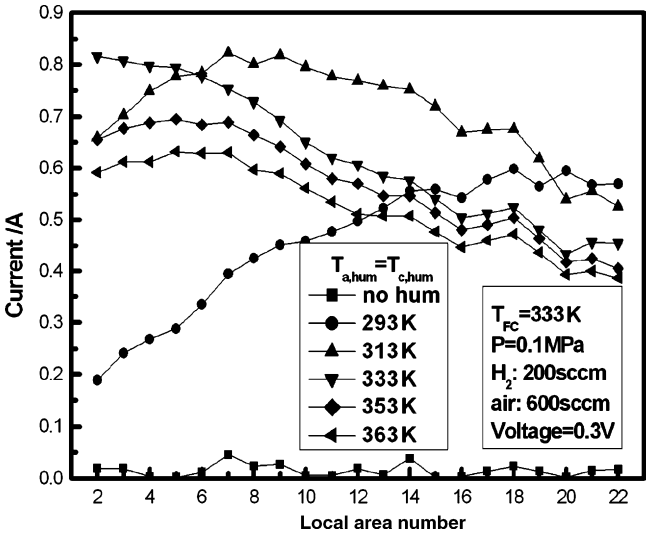

Fig. 15. Different patterns of local current distributions at different humidification temperatures.

increased progressively, causing the local current to increase; further down the stream, the membrane was well-hydrated and the effects of decreased reactant concentrations became dominant, causing the local currents to decrease. It can also be seen from Fig. 13 that the lower the cell voltage was, the earlier the maximum current was reached. This was due to the higher water generation rate at higher currents and faster consumption rate of the reactants. This set of experimental results shows the opposite effects of membrane hydration and reactant concentration reduction were at play. At the inlet, it was the membrane hydration that played the dominant role; at certain points, the two effects were equal and the local current reached its maximum; further down stream the effect of reactant concentration reduction became dominant.

Fig. 14 shows the local current distributions at different voltages when for humidification temperatures were 363 K, 30 K higher than the cell temperature of 333 K. The general trend for

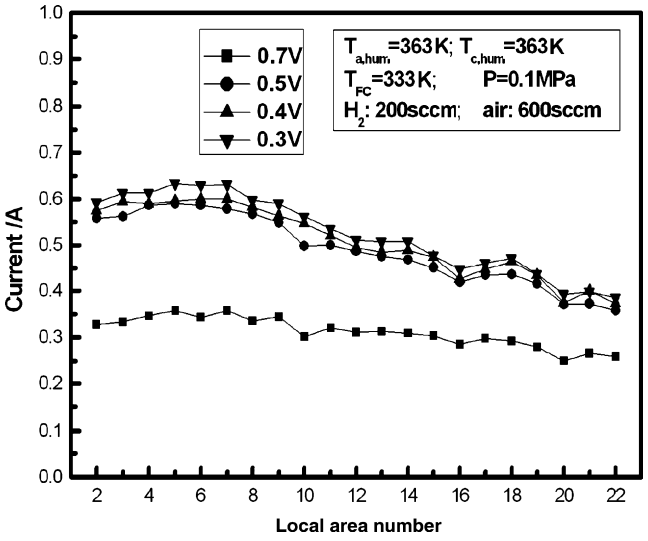

Fig. 14. Local current distributions at different cell voltages. Cell temperature is 333 K, and humidification temperatures at both sides are 363 K.

local currents for all the cases were decreasing along the channel, indicating a well-hydrated membrane and the decreases were caused by decreased reactant concentrations.

From Figs. 13–15, it can be seen that three distinctive patterns of current density distributions existed under different humidification temperatures. To put all the scenarios together, current distributions at different humidification temperatures are presented in Fig. 15. Note that for all the cases, the humidification temperature at the anode and cathode were the same. Generally, when the cell is highly under-humidified, the local current density increases monotonously along the channel; when the cell is moderately under-humidified, the local current density first increases, reach a maximum, and then decreases along the channel; when the cell is well-hydrated or over-hydrated, the local current decreases monotonically along the channel.

4. Conclusions

The technique of current density distribution measurement gasket [1] is applied to measure local current distribution in a PEM fuel cell with serpentine flow field at various humidification temperatures. The following conclusion can be drawn based on the experimental results:

- When the cathode is not humidified, the cell performance increases with anode humidification temperature, even when it is higher than the cell operating temperature.
- When the cathode is fully humidified, the cell performances are fairly well without anode humidification. The local current density increase with the anode humidification temperature till it reaches the cell temperature and decreases significantly when the anode humidification temperature is higher than the cell temperature, especially near the inlet.
- When the anode is not humidified, the local current density near the inlet increase with cathode humidification temperature; while the local current density downstream reaches its

maximum when the cathode humidification temperature is equal to the cell temperature.

- When the anode and cathode humidification temperatures are equal, if the cell is highly under-humidified, local current density starts very low and increases monotonously along the channel; if the cell is moderately under-humidified, the local current density first increases, reaches a maximum, and then decreases along the channel; when the cell is well-hydrated or over-hydrated, the local current decreases monotonically along the channel.

Acknowledgements

Financial support from the National Natural Science Foundation of China for Outstanding Young Oversees Chinese Scholar under contract 50228606 and the National Basic Research Program of China under contract 2003CB214500 are gratefully acknowledged.

References

[1] H. Sun, G.S. Zhang, L.J. Guo, H. Liu, J. Power Sources 158 (2006) 326–332.
[2] Ch. Wieser, A. Helmbold, E. Gulzow, J. Appl. Electrochem. 30 (2000) 803–807.
[3] J. Stumper, S.A. Campbell, D.P. Wilkinson, Electrochim. Acta 43 (24) (1998) 3773–3783.
[4] S.J. Cleghorn, C.R. Derouin, M.S. Wilson, S. Gotterfeld, J. Appl. Electrochem. 28 (1998) 663–672.
[5] D. Brett, S. Atkins, N. Brandon, V. Vesovic, N. Vasileiadis, A. Kucernak, Electrochem. Commun. 3 (2001) 628–632.
[6] A.B. Geiger, R. Eckl, A. Wokaun, G.G. Scherer, J. Electrochem. Soc. 151 (3) (2004) A394–A398.
[7] M. Noponen, T. Mennola, M. Mikkola, T. Hottinen, P. Lund, J. Power Sources 106 (2002) 304–312.
[8] M.M. Mench, C.Y. Wang, M. Ishikawa, J. Electrochem. Soc. 150 (8) (2003) A1052–A1059.
[9] A. Hakenjos, H. Muenter, U. Wittstadt, C. Hebling, J. Power Sources 131 (2004) 213–216.
[10] Z. Liu, Z. Mao, B. Wu, L. Wang, V.M. Schmidt, J. Power Sources 141 (2005) 205–210.
[11] N. Rajalakshmi, M. Raja, K.S. Dhathathreyan, J. Power Sources 112 (2002) 331–336.
[12] Z.H. Wang, C.Y. Wang, K.S. Chen, J. Power Sources 94 (2001) 40–50.
[13] L. You, H. Liu, Int. J. Heat Mass Trans. 45 (2002) 2277–2287.
[14] D. Natarajan, T.V. Nguyen, J. Power Sources 115 (2003) 66–80.
[15] M. Hu, A. Gu, M. Wang, X. Zhu, L. Yu, Energy Conserv. Manage. 45 (2004) 1861–1882.
[16] M. Hu, A. Gu, X. Zhu, M. Wang, A. Gu, L. Yu, Energy Conserv. Manage. 45 (2004) 1833–1916.
[17] H. Sun, H. Liu, L.J. Guo, J. Power Sources 143 (2005) 125–135.